Consistent Modeling of Capacitances and Transit Times of GaAs-Based HBTs

Matthias Rudolph, *Member, IEEE,* and Ralf Doerner, *Member, IEEE*

***Abstract*—This paper investigates how time delays and capacitances observed under small-signal conditions can be consistently accounted for in heterojunction bipolar transistor (HBT) large-signal models. The approach starts at the circuit level by mapping the large-signal equivalent circuit (which consists of charge and current sources) to the well-known small-signal circuit (which consists of capacitances, transit-time, and resistances). It is shown that and how bias dependent charge sources at either pn-junction impact transit-time, base–collector capacitance, and their mutual dependence. It is demonstrated for the example of a GaAs-based HBT that the interrelation of the elements is observed in measurements as predicted. The results of the investigation enhance understanding of HBT model characteristics and provide a criterion to check model consistency.**

***Index Terms*—Equivalent circuit, heterojunction bipolar transistor (HBT), semiconductor device modeling.**

I. Introduction

An accurate description of transit times is crucial for HBT model performance. This is especially true for GaAs- and InP-based HBTs, where the transit frequency f_t depends strongly on bias point. It is a function of collector–base voltage as well as collector current. One reason is velocity modulation of the electrons in the collector space–charge region, which is effective at lower current densities. It is caused by the nonlinear dependence of electron mobility on the electric field in GaAs and InP [1]. At higher current densities, base push-out occurs and leads to drastically increased transit times. These effects have been identified to be an important source of nonlinear distortion [2], [3]. But not only transit time τ_f is a function of voltage and current, the same applies to the base-collector capacitance $C'_{\rm bc}$.

These small-signal quantities are caused by storage of charges in the bulk neutral base, and the base-collector space–charge region. Basically, storage of a charge Q due to collector current I_c results in a time-delay

$$\tau_f = \frac{\partial Q}{\partial I_c} \tag{1}$$

while storage of charge due to base-collector voltage $V_{\rm bc}$ results in a capacitance [4], [5]

$$C'_{\rm bc} = \frac{\partial Q}{\partial V_{\rm bc}}. \tag{2}$$

In this paper, τ_f and $C'_{\rm bc}$ denote the forward transit time and base–collector capacitance in general, respectively, without a strict link to an element of a specific equivalent circuit. The interdependence of transit-time and capacitance was discussed in the small-signal domain and explained from HBT physics recently [1], [6]–[9].

When formulating an equivalent-circuit based large-signal model, one faces two main challenges concerning the storage of charge.

1) The charge stored in the bulk material of the three-terminal transistor has to be split and represented by two-terminal branch charges in the equivalent circuit.
2) The total derivative of the charge sources must yield the desired small-signal capacitances and time delays.

Compact models for bipolar transistors rely on two charge sources, $Q_{\rm be}$ between base and emitter node, and $Q_{\rm bc}$ between base and collector node. Each charge will result in a capacitance and a time constant in the small-signal equivalent circuit. Therefore, it is not possible to formulate a large-signal model describing only one of the small-signal elements without affecting some others, too. The choice of the formulas for $Q_{\rm be}$ and $Q_{\rm bc}$ determines not only the values, but also the bias dependence of the interrelated small-signal equivalent circuit elements.

In contrast to FET models, the implications of charge models are unfortunately only sparsely addressed, even in case of highly accurate HBT models. The respective publications rather discuss the results obtained for the key parameter—usually the total transit time—but do not mention the impact on the other small-signal parameters.

It is the aim of this paper to shed light on this blind spot by addressing two important issues concerning the formulation of large-signal HBT models:

1) The HBT large-signal model must yield S-parameters identical to those of the common small-signal models. However, the current gain of the small-signal HBT model is dispersive, while the linearized large-signal equivalent circuit elements are constant over frequency. Therefore, any frequency dispersive element would have to be approximated by appropriate nondispersive circuitry, e.g., an excess-phase network [10]. On the other hand, a charge being a function of multiple voltages will result in transcapacitance elements in the linearized equivalent circuit. These are not present in the small-signal model. Since both models are accurate descriptions of the same device, one has to clarify under which conditions and to what extent the two descriptions can be considered equivalent. At the same time, the implication of splitting the bulk charge Q and representing it by branch charges is to be addressed.

Manuscript received March 18, 2005; revised June 6, 2005. The review of this paper was arranged by Editor C.-P. Lee.

The authors are with the Ferdinand-Braun-Institut für Höchstfrequenztechnik (FBH), Berlin D-12489, Germany (e-mail: rudolph@fbh-berlin.de).

Digital Object Identifier 10.1109/TED.2005.854284

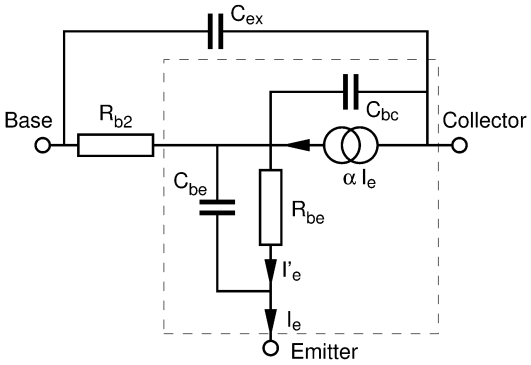

Fig. 1. Standard intrinsic HBT small-signal equivalent circuit. The active transistor is shown inside the dashed box. The elements R_{b2} and $C_{\rm ex}$ describe the parasitic base-collector diode due to the mesa structure and will be omitted in the following.

2) Since capacitances and time delays result from a common charge, they are interdependent in value and bias dependence, as follows from (1) and (2). This interrelation has an impact on the degrees of freedom one has regarding the formulation of a model. It will be shown that the interdependence can be validated by measurement data. Hence, one has to make sure that it is described correctly by any circuit-based HBT model.

In Sections II and III, these two issues will be addressed subsequently. The implementation in dedicated HBT models will be addressed, and the findings will be verified comparing measurement and simulation data of an InGaP/GaAs HBT.

II. Consistency of Small-Signal and Linearized Large-Signal Equivalent Circuits

In this section, we will show how the linearized large-signal equivalent circuit, despite its different topology, can be understood as close approximation of the common small-signal equivalent circuit. The investigation focuses only on the intrinsic elements, after deembedding of the parasitics.

Fig. 1 presents the intrinsic small-signal equivalent circuit of an HBT in T-topology. In the following, we will concentrate on the model for the active part of the HBT, shown inside the dashed box. For sake of completeness, also the two parasitic elements describing the mesa structure of the device are shown in this figure. These are $C_{\rm ex}$ which is the capacitance of the reverse biased parasitic base-collector diode, and the intrinsic resistance R_{b2} which describes the resistance of the base region. Commonly, the resistances of the reverse biased intrinsic and extrinsic base–collector diodes are large enough to be neglected.

The current gain α used in this equivalent circuit is dispersive, since it shows a time-delay τ_α and a low-pass characteristic with a corner frequency ω_α

$$\alpha = \frac{\alpha_0 e^{-j\omega\tau_\alpha}}{1 + j\frac{\omega}{\omega_\alpha}}. \tag{3}$$

The corresponding large-signal equivalent circuit for the active HBT shown in Fig. 2 is based on charges instead of capacitances and on currents instead of resistances [11]–[15]. Small-signal resistances are modeled by diode current–voltage

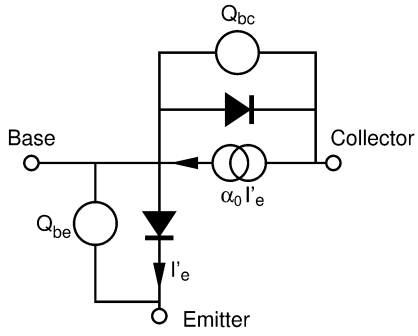

Fig. 2. Intrinsic HBT large-signal equivalent circuit.

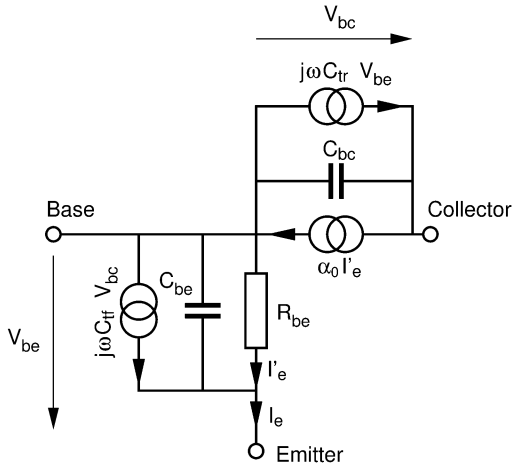

Fig. 3. Intrinsic HBT small-signal equivalent circuit derived from the circuit shown in Fig. 2. $V_{\rm bc}$ denotes the base–collector voltage and $V_{\rm be}$ the base–emitter voltage.

(I–V) characteristics for the base–emitter and base–collector pn-junction. The current gain is set to a constant value α_0, since the large-signal model has to be defined in the time domain. The contribution of the nonlinear charges is more involved, and needs to be discussed in greater detail. In the general case, both charges $Q_{\rm be}$ and $Q_{\rm bc}$ are functions of base–emitter and base–collector voltages $V_{\rm be}$ and $V_{\rm bc}$. Hence, the small-signal current through the charge sources is given by

$$\begin{aligned} i'_{\rm be} &= \left.\frac{\partial Q_{\rm be}}{\partial V_{\rm be}}\right|_{V_{\rm BE}} j\omega v_{\rm be} + \left.\frac{\partial Q_{\rm be}}{\partial V_{\rm bc}}\right|_{V_{\rm BC}} j\omega v_{\rm bc} \\ &= j\omega C_{\rm be} v_{\rm be} + j\omega C_{\rm tf} v_{\rm bc} \end{aligned} \tag{4}$$

$$\begin{aligned} i'_{\rm bc} &= \left.\frac{\partial Q_{\rm bc}}{\partial V_{\rm be}}\right|_{V_{\rm BE}} j\omega v_{\rm be} + \left.\frac{\partial Q_{\rm bc}}{\partial V_{\rm bc}}\right|_{V_{\rm BC}} j\omega v_{\rm bc} \\ &= j\omega C_{\rm tr} v_{\rm be} + j\omega C_{\rm bc} v_{\rm bc} \end{aligned} \tag{5}$$

where $V_{\rm BE}$, $V_{\rm BC}$ denote the dc bias point, and $v_{\rm be}$, $v_{\rm bc}$ are the small-signal amplitudes of the voltages $V_{\rm be}$, $V_{\rm bc}$, respectively. The two elements $C_{\rm tf}$ and $C_{\rm tr}$ are transcapacitances, i.e., voltage-controlled current sources, as shown in Fig. 3. In the following, it will be discussed how the linearized large-signal equivalent circuit can be understood in terms of the small-signal circuit shown in Fig. 1.

In doing so we first substitute the current I'_e driving the current gain α, and $V_{\rm be}$ driving the transcapacitance $C_{\rm tr}$ by the total

emitter current I_e (see Fig. 3) that corresponds to the driving I_e current in the small-signal equivalent circuit (Fig. 1)

$$V_{\rm be} = \frac{R_{\rm be}}{1+j\omega\tau_{\rm be}}\left(I_e - j\omega C_{\rm tf} V_{\rm bc}\right) \tag{6}$$

$$I_e' = \left(\frac{1}{1+j\omega\tau_{\rm be}}\right) I_e - \left(\frac{j\omega C_{\rm tf}}{1+j\omega\tau_{\rm be}}\right) V_{\rm bc} \tag{7}$$

with $\tau_{\rm be} = C_{\rm be}R_{\rm be}$. It is now possible to write the total current I_c through the base–collector branch as a function of $V_{\rm bc}$ and I_e

$$\begin{aligned} I_c &= j\omega C_{\rm bc} V_{\rm bc} + j\omega C_{\rm tr} V_{\rm be} - \alpha_0 I_e' \\ &= j\omega\left(C_{\rm bc} + \frac{\alpha_0 C_{\rm tf} - j\omega C_{\rm tf} C_{\rm tr} R_{\rm be}}{1+j\omega\tau_{\rm be}}\right) V_{\rm bc} \\ &\quad - \left(\frac{\alpha_0 - j\omega R_{\rm be} C_{\rm tr}}{1+j\omega\tau_{\rm be}}\right) I_e. \end{aligned} \tag{8}$$

The first component of this current can be understood as effective capacitance, and the second one as an effective current gain in terms of the small-signal equivalent circuit

$$I_c = j\omega C_{\rm bc,eff} V_{\rm bc} - \alpha_{\rm eff} I_e \tag{9}$$

with

$$C_{\rm bc,eff} = C_{\rm bc} + \frac{\alpha_0 C_{tf} - j\omega C_{\rm tf} C_{\rm tr} R_{\rm be}}{1+j\omega\tau_{\rm be}} \tag{10}$$

$$\alpha_{\rm eff} = \frac{\alpha_0 - j\omega\tau_c}{1+j\omega\tau_{\rm be}} \tag{11}$$

with $\tau_c = C_{\rm tr}R_{\rm be}$. Concerning $\alpha_{\rm eff}$, it was shown in [4] and [10] that this formula is a suitable approximation of α in (3) in the frequency range of practical interest, since the expression $\alpha_0 - j\omega\tau_c$ can be understood as the first order approximation of a time delay $\alpha_0 e^{-j\omega\tau_c}$.

It should be emphasized at this point that the model as shown in Fig. 2 can be called "quasi-static" since none of the sources is controlled by a time-delayed voltage, as, for example, in case of the model proposed in [16]. On the other hand, the same equivalent circuit can result from a "nonquasi-static" physical consideration. This is the case, e.g., for the approach called "charge partitioning," which assigns the base charge partly to $Q_{\rm be}$ and $Q_{\rm bc}$ [12], [13]. Therefore, the "quasi-static" circuit model can describe also a strictly speaking "nonquasi-static" physics-based model.

As shown in (10), $C_{\rm bc,eff}$ becomes dispersive due to $C_{\rm tf}$. However, in the lower frequency range with $\omega C \ll 1$ and $\omega\tau_{\rm be} \ll 1$, $C_{\rm bc,eff} = C_{\rm bc} + \alpha_0 C_{\rm tf}$ holds.

While $C_{\rm tr}$ can be fully absorbed into the effective current gain $\alpha_{\rm eff}$ [see (11)], the second transcapacitance, $C_{\rm tf}$, mainly results in a modification of $C_{\rm bc,eff}$ but it cannot be fully removed from the equivalent circuit.

This becomes clear when considering the Y-parameters for the equivalent circuit of Fig. 3

$$Y_{11} = j\omega[C_{\rm tf} + C_{\rm bc} + C_{\rm be} + C_{\rm tr}] + \frac{(1-\alpha_0)}{R_{\rm be}} \tag{12}$$

$$Y_{12} = -j\omega[C_{\rm bc} + C_{\rm tf}] \tag{13}$$

$$Y_{21} = \frac{\alpha_0}{R_{\rm be}} - j\omega[C_{\rm bc} + C_{\rm tr}] \tag{14}$$

$$Y_{22} = j\omega C_{\rm bc}. \tag{15}$$

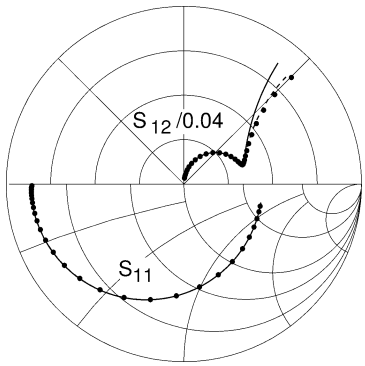

Fig. 4. S-parameters S_{11} and S_{12}, simulated with different intrinsic HBT equivalent circuits, $f = 50$ MHz–50 GHz. The model parameters are: $R_{b2} = 4\Omega$, $R_{\rm be} = 1.25\Omega$, $C_{\rm ex} = 20$ fF, $C_{\rm bc} = 30$ fF, $\tau_c = 2$ ps, $\tau_{\rm be} = 4$ ps, $C_{\rm be} = \tau_{\rm be}/R_{\rm be}$. (Symbols) Equivalent circuit of Fig. 1, (dotted lines) collector time delay replaced by BC-transcapacitance ($C_{\rm tr} = \tau_c$), (solid lines) BC- and BE-transcapacitances ($C_{\rm tf} = 10$ fF, $C_{\rm bc} = 20$ fF).

As can be seen, the sum of $C_{\rm bc}$ and $C_{\rm tf}$ is found only in Y_{11} and Y_{12}, but not in Y_{21} and Y_{22}. This difference might appear to be of merely academic interest, but this is not true since it affects parameter extraction from measurement data. It is common to extract the total base-collector capacitance of the small-signal equivalent circuit (Fig. 1) by [17]

$$C_{\rm bc} + C_{\rm ex} = \frac{1}{\omega}{\rm Im}\left\{\frac{-1}{Z_{21} - Z_{22}}\right\}. \tag{16}$$

In the case of the equivalent circuit Fig. 3, $C_{\rm ex}$ is known and deembedded beforehand. Due to the two additional elements $C_{\rm tf}$ and $C_{\rm tr}$, (16) without $C_{\rm ex}$ reads

$$\begin{aligned} \left\{\frac{-1}{Z_{21} - Z_{22}}\right\} &= j\omega C_{\rm bc}\left(\frac{1+j\omega C_{\rm be}R_{\rm be}}{1+j\omega\left(C_{\rm be}+C_{tf}\right)R_{\rm be}}\right) \\ &\quad + j\omega C_{\rm tf}\left(\frac{\alpha_0 - j\omega C_{\rm tr}R_{\rm be}}{1+j\omega\left(C_{\rm be}+C_{\rm tf}\right)R_{\rm be}}\right). \end{aligned} \tag{17}$$

For typical values of capacitances, $\omega C \ll 1$, and $\alpha_0 \approx 1$, the terms in brackets on the right-hand side of this equation approach unity in the lower frequency range. Therefore, we obtain

$$\frac{1}{\omega}{\rm Im}\left\{\frac{-1}{Z_{21} - Z_{22}}\right\} \approx C_{\rm bc} + C_{\rm tf}. \tag{18}$$

This result is similar to the one obtained for $C_{\rm bc,eff}$, (10), above. The differences result in the fact that, in the first case, the base-collector branch was treated isolated, while now, the full equivalent circuit is considered.

To highlight the effect of $C_{\rm tf}$, Figs. 4–6 present small-signal simulation data. Three simulations are performed, one with the equivalent circuit shown in Fig. 1 (symbols), a second one with the time delay replaced by a base–collector transcapacitance $C_{\rm tr}$ (dashed lines), and the third one with an additional base-emitter transcapacitance $C_{\rm tf}$ (solid lines). In the last case, $C_{\rm bc}$ was reduced by the value of $C_{\rm tf}$. The equivalent circuit parameters are given in the caption of Fig. 4. Differences in the S-parameters are in this case only observed in S_{22} beyond the kink, which is at 6 GHz in all simulations. The arrow in Fig. 5 denotes the point where the simulation with the element $C_{\rm tf}$ reaches 50 GHz, which is close to S_{22} at 30 GHz simulated with the two other

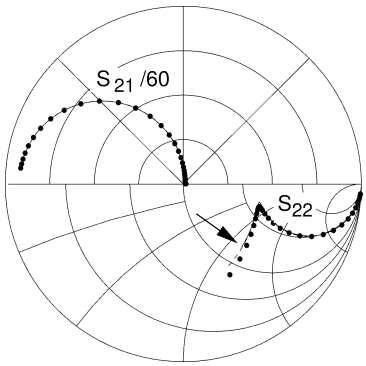

Fig. 5. S_{21} and S_{22} (other data as in Fig. 4). The arrow denotes the value $f = 50$ GHz obtained with the equivalent circuit with BC- and BE-transcapacitances ($f = 30$ GHz for the other equivalent circuits).

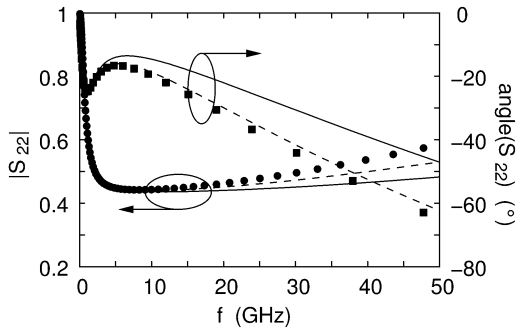

Fig. 6. S_{22} from Fig. 5 plotted as magnitude and phase against frequency. (Symbols) Equivalent circuit of Fig. 1, (dashed lines) collector time delay replaced by BC-transcapacitance, (solid lines) BC- and BE-transcapacitances.

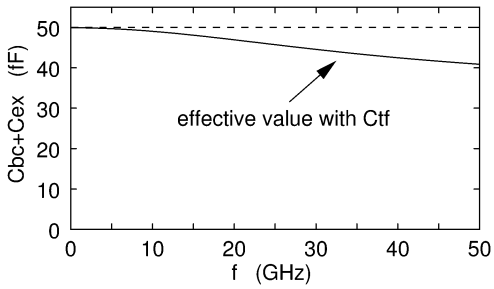

Fig. 7. Total $C_{\rm bc}+C_{\rm ex}$ as extracted by (16) from simulations shown in Figs. 4 and 5. (Dashed line) $C_{\rm bc} = 30$ fF, $C_{\rm ex} = 20$ fF. (Solid line) effective value with transcapacitance $C_{\rm tf} = 10$ fF, $C_{\rm bc} = 20$ fF, $C_{\rm ex} = 20$ fF.

topologies. The differences are better observed when plotting S_{22} as a function of frequency; see Fig. 6.

Fig. 7 shows the capacitance value as extracted from the simulated Z-parameters by means of (16). As expected, in the ideal case, the value $C_{\rm bc} + C_{\rm ex} = 50$ fF is obtained. For the solid line, $C_{\rm tf} = 10$ fF is added, and $C_{\rm bc}$ is reduced by this value. As expected from (17), the extracted capacitance is dispersive, with a low-frequency value of 50 fF.

Summarizing we can state that the effective base–collector capacitance $C_{\rm bc,eff}$ is determined by $C_{\rm bc}$, but also by $C_{\rm tf}$. This result is important since it shows that the charge function Q can be assigned either to the base–emitter or the base–collector branch. Both formulations can be distinguished in measured data only at high frequencies around f_t. This results in an additional degree of freedom in formulating a model, since the charge function can be assigned partly to $Q_{\rm be}$ and partly to $Q_{\rm bc}$. While both descriptions are quite similar at low frequencies, differences increase with frequency. Thus, the partition of charges can be used to fine-tune the RF behavior of the model.

However, the Q description is important also because it determines the interdependence of the small-signal elements $C'_{\rm bc}$ and τ_f. This will be treated in Section III.

III. Interdependence of HBT Capacitances and Transit Times

As was shown in Section II, a charge $Q_{\rm bx}$ can be located at either base–collector or base-emitter branch of a large-signal model, as $Q_{\rm bc}$ or $Q_{\rm be}$, respectively. In both cases, it gives rise to small-signal capacitance $C_{\rm bcx} = \partial Q_{\rm bx}/\partial V_{\rm bc}$, and transit time $\tau_x = \partial Q_{\rm bx}/\partial I_e = (\partial Q_{\rm bx}/\partial V_{\rm be})(\partial V_{\rm be}/\partial I_e)$. In this section, τ_x denotes the transit-time component to be modeled, being either $\tau_{\rm be}$ or τ_c as defined above. The same applies to the voltage-derivative of the respective charge, $C_{\rm bcx}$, which contributes to $C_{\rm bc,eff}$.

This section addresses the interrelation of capacitance and time-delay values and bias-dependencies due to the fact that they originate from the same charge formula. Regarding measurement-extracted data of a state-of-the-art GaAs HBT it will be shown that the mathematical interdependence of the model parameters reflects the physical behavior of the device.

Regarding bias dependence of transit time and thus cutoff frequency f_t in III–V HBTs, the following two main regions can be distinguished:

1) at lower currents and higher voltages, f_t increases with current ($C'_{\rm bc}$, τ_f decrease),
2) at higher currents and lower voltages, f_t decreases with current ($C'_{\rm bc}$, τ_f increase).

The first effect, sometimes called f_t-peaking, is due to velocity modulation in the collector space-charge region. It is therefore usually modeled using the base-collector charge source $Q_{\rm bc}$ [4], [15]. The other one is due to base push-out or even quasi-saturation and usually is modeled employing the base-emitter charge source $Q_{\rm be}$ [11], [14], [15]. The latter model often is motivated only by the increase of τ_f, without mentioning the impact on $C'_{\rm bc}$ at all. Fig. 8 shows τ_f and $C'_{\rm bc}$ as functions of I_c and $V_{\rm ce}$. Device under test is a 3×30 μm^2 InGaP/GaAs HBT from the FBH $4''$ process line [18]. The main layer structure consists of a 30-nm InGaP n-doped ($3 \cdot 10^{17}$ cm^{-3}) emitter, a 100-nm uniformly doped ($4 \cdot 10^{19}$ cm^{-3}) p-GaAs base, a 1-μm GaAs collector (n-doped, $2 \cdot 10^{16}$ cm^{-3}), and a 700-nm-thick n^+-GaAs subcollector ($5 \cdot 10^{18}$ cm^{-3}). The values are extracted from measured (left) and simulated (right) S-parameters with an analytical extraction algorithm [19].

As discussed in Section II, τ_f and $C'_{\rm bc}$ are not independent of each other. In case of velocity modulation, i.e., case 1, the following interrelations are observed:

$$C_{\rm bcx} = \frac{\partial Q_{\rm bx}}{\partial V_{\rm bc}} > 0 \qquad \tau_x = \frac{\partial Q_{\rm bx}}{\partial I_e} > 0$$

$$\frac{\partial C_{\rm bcx}}{\partial I_e} = \frac{\partial^2 Q_{\rm bx}}{\partial V_{\rm bc}\partial I_e} < 0 \Rightarrow \frac{\partial \tau_x}{\partial V_{\rm bc}} = \frac{\partial^2 Q_{\rm bx}}{\partial I_e \partial V_{\rm bc}} < 0$$

$$\frac{\partial C_{\rm bcx}}{\partial V_{\rm bc}} = \frac{\partial^2 Q_{\rm bx}}{\partial V_{\rm bc}^2} > 0 \qquad \frac{\partial \tau_x}{\partial I_e} = \frac{\partial^2 Q_{\rm bx}}{\partial I_e^2} < 0. \quad (19)$$

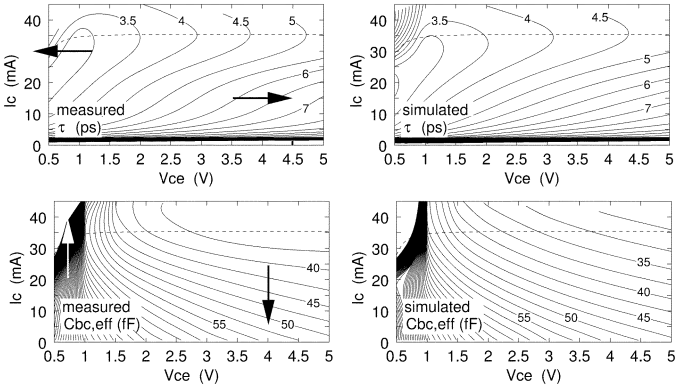

Fig. 8. Values of $C'_{\rm bc}$ and τ_f, (left) extracted from measured and (right) simulated S-parameters.

This behavior is shown in Fig. 8 for $V_{\rm ce} = 4\,{\rm V}$, $I_c = 15\,{\rm mA}$ by the arrows which indicate a positive slope for $\partial\tau_f/\partial V_{\rm bc}$ and $\partial C'_{\rm bc}/\partial I_e$. Please note that $V_{\rm ce} \propto -V_{\rm bc}$, and $I_c \approx I_e$.

The recent generation of HBT models, e.g., the Agilent [15] and FBH [20] models, account for the mutual dependence of τ_f and $C'_{\rm bc}$ by providing a unified charge formula. However, even though it is the benefit of the UCSD model [21] to account for the velocity modulation effects comprehensively for the first time, this interdependence is not accounted for. Hence, two sets of model parameters are provided which give the impression that the current–dependence of τ_f and $C'_{\rm bc}$ can be controlled independently. In reality, however, the two respective charge formulas add up and disturb each other while trying to describe the same effect. A recent approach decouples τ_f and $C'_{\rm bc}$, by relying on nonlinear capacitances instead of charges [22]. However, this comes at the cost of giving up charge conservation for the base–emitter and base–collector branches.

The simulations shown in Fig. 8 are performed using the FBH model. The formula employed for $Q_{\rm bc}$ is slightly varied compared to the previously published one in [4] in order to gain higher flexibility

$$Q_{\rm bc} = \underbrace{[1-\tanh(\xi)]}_{f(I_c)} \cdot \underbrace{[Q_c + (1-X_{J0})C_{\rm min}V_{\rm bc}]}_{g(V_{\rm bc})} + \underbrace{X_{J0}C_{\rm min}V_{\rm bc}}_{h(V_{\rm bc})} \quad (20)$$

with

$$Q_c = -(C_{jc0}-C_{\rm min})\phi\frac{\left(\frac{1-V_{\rm bc}}{\phi}\right)^{1-m}}{1-m} \quad (21)$$

$$\xi = \frac{I_c}{2I_0} + \left(\frac{I_c}{2I_0}\right)^{k_{jc}}. \quad (22)$$

Q_c is the usual equation describing the charge of a space–charge region, and the additional parameters are a minimum capacitance value $C_{\rm min}$ which is reached at the current limit I_0. X_{J0} and $k_{\rm jc}$ are parameters that control the slope of $Q_{\rm bc}$ with current. The argument in [4] started from the approximately linear slope of $C_{\rm bc}$ with collector current, therefore the charge description is based on the depletion capacitance formula.

In order to determine $C_{\rm bc}$ and τ_c, the function $Q_{\rm bc}$ will be split into three terms which depend only on I_c or on $V_{\rm bc}$, as indicated in (20)

$$Q_{\rm bc}(I_c, V_{\rm bc}) = f(I_c)\cdot g(V_{\rm bc}) + h(V_{\rm bc}). \quad (23)$$

The derivatives with respect to I_c and $V_{\rm bc}$ are defined as $f' = df(I_c)/dI_c$, $g' = dg(V_{\rm bc})/dV_{\rm bc}$, and $h' = dh(V_{\rm bc})/dV_{\rm bc}$

$$f' = \frac{-1}{\cosh^2(\xi)}\left[\frac{1}{2I_0} + \frac{k_{jc}}{2I_0}\left(\frac{I_c}{2I_0}\right)^{k_{jc}-1}\right] \quad (24)$$

$$g' = \frac{C_{jc0}-C_{\rm min}}{\left(\frac{1-V_{\rm bc}}{\phi}\right)^m} + (1-X_{j0})C_{\rm min} \quad (25)$$

$$h' = X_{j0}C_{\rm min}. \quad (26)$$

The small-signal values now read

$$C_{\rm bc} = \frac{\partial Q_{\rm bc}}{\partial V_{\rm bc}} = f(I_c)\cdot g'(V_{\rm bc}) + h'(V_{\rm bc}) \quad (27)$$

$$\tau_c = \frac{\partial Q_{\rm bc}}{\partial I_c} = f'(I_c)\cdot g(V_{\rm bc}) \quad (28)$$

$$\frac{\partial C_{\rm bc}}{\partial I_c} = \frac{\partial \tau_c}{\partial V_{\rm bc}} = f'(I_c)\cdot g'(V_{\rm bc}). \quad (29)$$

This shows that τ_c increases with $V_{\rm ce} \propto -V_{\rm bc}$, and $C_{\rm bc}$ decreases with I_c, since $f'(I_c) < 0$ and $g'(V_{\rm bc}) > 0$.

Under base push-out condition, on the other hand, the main focus is on the reduction of f_t with increasing current. Therefore, it is traditionally modeled by an appropriate function of $Q_{\rm be}$, by integrating τ_f [11]. However, especially near saturation, τ_f strongly depends on voltage, too, which results in a slope in $C'_{\rm bc}$. This is indicated by the arrows in Fig. 8 for $V_{\rm ce} = 0.7\,{\rm V}$, $I_c = 27\,{\rm mA}$. In this region, which corresponds to case 2 mentioned above, one has

$$\tau_x = \frac{\partial Q_{\rm bx}}{\partial I_e} > 0 \qquad C_{\rm bcx} = \frac{\partial Q_{\rm bx}}{\partial V_{\rm bc}} > 0$$

$$\frac{\partial \tau_x}{\partial V_{\rm bc}} = \frac{\partial^2 Q_{\rm bx}}{\partial I_e \partial V_{\rm bc}} > 0 \Rightarrow \frac{\partial C_{bcx}}{\partial I_e} = \frac{\partial^2 Q_{\rm bx}}{\partial V_{\rm bc}\partial I_e} > 0$$

$$\frac{\partial \tau_x}{\partial I_e} = \frac{\partial^2 Q_{\rm bx}}{\partial I_e^2} > 0 \qquad \frac{\partial C_{\rm bcx}}{\partial V_{\rm bc}} = \frac{\partial^2 Q_{\rm bx}}{\partial V_{\rm bc}^2} > 0. \quad (30)$$

The formula employed for this region is taken from HICUM [14]. Although this model was derived for Si-based transistors, its $Q_{\rm be}$ description is suited for III–V HBTs, too [15]. The model will be recalled here only shortly. Refer to [14, (28)–(35) and (45), (46)] for the full derivation. The charge is given by current I_c and the width of the base push-out region w is given by

$$Q_{\rm be,x} = t_{\rm hcs} I_c w^2 \quad (31)$$

$$w = \frac{i_x + \sqrt{i_x^2 + a_{\rm hc}}}{1+\sqrt{1+a_{\rm hc}}} \quad (32)$$

with

$$i_x = 1 - \frac{I_{\rm CK}}{I_c}. \quad (33)$$

$t_{\rm hcs}$ and $a_{\rm hc}$ are parameters, and $I_{\rm CK}$ is the current that defines the onset of base push-out. It is given by

$$I_{\rm CK} = \frac{V_{\rm ceff}}{r_{\rm ci0}\sqrt{1+\left(\frac{V_{\rm ceff}}{V_{\rm lim}}\right)^2}}\left[1+\frac{x+\sqrt{x^2+10^{-3}}}{2}\right] \quad (34)$$

with $x = (V_{\rm ceff} - V_{\rm lim})/V_{\rm PT}$, and the parameters $r_{\rm ci0}$, $V_{\rm lim}$, and $V_{\rm PT}$. The voltage $V_{\rm ceff}$ is an effective collector-emitter voltage, which is limited to positive values and shifted compared to $V_{\rm ce}$. Within this discussion, we set $dV_{\rm ceff}/dV_{\rm bc} \approx -1$.

The transit-time $\tau_{\rm be} = \partial Q_{\rm be,x}/\partial I_c$ and capacitances $C_{\rm bcx} = \partial Q_{\rm be,x}/\partial V_{\rm bc}$ become

$$\tau_{\rm be} = t_{\rm hcs} w^2 \left(1+\frac{2I_{\rm CK}}{I_c\sqrt{i_x^2+a_{\rm hc}}}\right) \quad (35)$$

$$C_{bcx} = 2t_{\rm hcs} w^2 \left(\frac{-\left(\frac{dI_{\rm CK}}{dV_{\rm bc}}\right)}{\sqrt{i_x^2+a_{\rm hc}}}\right). \quad (36)$$

The variation of $C'_{\rm bc}$ with current is modeled indirectly, since it results only from the voltage dependence of $I_{\rm CK}$. Since $I_{\rm CK} \approx V_{\rm ce}/r_{\rm ci0} \propto -V_{\rm bc}/r_{\rm ci0}$ at low voltages, τ_f increases with $V_{\rm bc}$, and $C'_{\rm bc}$, in turn, increases with I_c.

IV. Conclusion

It is the aim of the paper to clarify if and how large-signal III–V HBT models are able to account for the bias dependence of $C'_{\rm bc}$ and transit time τ_f at velocity modulation and base push-out conditions. From the results, the following conclusions can be drawn.

- The theoretical treatment reveals that a charge source $Q = f(V_{\rm be}, V_{\rm bc})$ always impacts both $C'_{\rm bc}$ and τ_f, since they result from the partial derivatives of Q. Q may be attributed either to the base-emitter junction as $Q_{\rm be}$ or to the base-collector junction as $Q_{\rm bc}$. This justifies model approaches that allow the user to freely partition the charges between the junctions, e.g., [15].
- Based on experimental data it is demonstrated that, in order to obtain an accurate model for $C'_{\rm bc}$ and τ_f, two functions are sufficient to describe the charge sources. One of the functions describes the effect of velocity modulation, the other one the base push-out effect.
- The interrelation between $C'_{\rm bc}$ and τ_f can be used as a criterion to assess model consistency. As described in Section III, not all of the common HBT models are consistent in this regard.

Acknowledgment

The author would like to thank the material and process technology departments of the FBH for providing the HBTs, S. Schulz for performing measurements, and Dr. W. Heinrich for helpful discussions and continuous encouragement.

References

[1] L. H. Camnitz and N. Moll, "An analysis of the behavior of microwave heterostructure bipolar transistors," in *Compound Semiconductor Transistors—Physics and Technology*, S. Tiwari, Ed. Piscataway, NJ: IEEE Press, 1993, pp. 21–45.

[2] M. Iwamoto, P. M. Asbeck, T. S. Low, C. P. Hutchinson, J. B. Scott, A. Cognata, X. Quin, L. H. Camnitz, and D. C. D'Avanzo, "Linearity characteristics of GaAs HBTs and the influence of collector design," *IEEE Trans. Microw. Theory Tech.*, vol. 48, no. 12, pp. 2377–2386, Dec. 2000.

[3] M. Rudolph and R. Doerner, "Large-signal HBT model requirements to predict nonlinear behavior," in *IEEE MTT-S Dig.*, 2004, pp. 43–46.

[4] M. Rudolph, R. Doerner, K. Beilenhoff, and P. Heymann, "Unified model for collector charge in heterojunction bipolar transistors," *IEEE Trans. Microw. Theory Tech.*, vol. 50, no. 7, pp. 1747–1751, Jul. 2002.

[5] D. E. Root, M. Iwamoto, and J. Wood, "Device modeling for III–V semiconductors—An overview," in *Proc. IEEE Compound Semicond. Integrated Circ. Symp.*, 2004, pp. 279–282.

[6] Y. Betser and D. Ritter, "Reduction of the base-collector capacitance in InP/GaInAs heterojunction bipolar transistors due to electron velocity modulation," *IEEE Trans. Electron Devices*, vol. 46, no. 4, pp. 628–633, Apr. 1999.

[7] M. Rohner, B. Willén, and H. Jäckel, "Velocity modulation in III/V-HBTs," *IEEE Trans. Electron Devices*, vol. 50, no. 5, pp. 1205–1213, May 2003.

[8] R. v. d. Toorn, J. C. J. Paasschens, and R. J. Havens, "A physically based analytical model of the collector charge of III–V heterojunction bipolar transistors," in *Dig. GaAs IC Symp.*, 2003, pp. 111–114.

[9] R. v d Toorn, J. C. J. Paasschens, and R. J. Havens, "Physically based analytical modeling of base-collector charge, capacitance and transit time of III–V HBTs," in *Proc. IEEE Compound Semicond. Integrated Circ. Symp.*, 2004, pp. 283–286.

[10] M. Rudolph, F. Lenk, R. Doerner, and P. Heymann, "Toward a unified method to implement transit-time effects in Pi-Topology HBT compact models," in *IEEE MTT-S Int. Microw. Symp. Dig.*, 2002, pp. 997–1000.

[11] I. E. Getreu, *Modeling the Bipolar Transistor*. Amsterdam, The Netherlands: Elsevier, 1978.

[12] H. Klose and A. W. Wieder, "The transient integral charge control relation—A novel formulation of the currents in a bipolar transistor," *IEEE Trans. Electron Devices*, vol. ED-34, no. 5, pp. 1090–1099, May 1987.

[13] J. C. J. Paasschens, W. J. Kloosterman, and R. v. d. Toorn. Model Derivation of MEXTRAM 504. Koninklijke Philips Electronics N.V., Nat.Lab. [Online]. Available: http://www.semiconductors.philips.com/Philips_Models/bipolar/mextram/index.html

[14] M. Schröter and T.-Y. Lee, "Physics-based minority charge and transit time modeling for bipolar transitors," *IEEE Trans. Electron Devices*, vol. 46, no. 2, pp. 288–300, Feb. 1999.

[15] M. Iwamoto, D. E. Root, J. B. Scott, A. Cognata, P. M. Asbeck, B. Hughes, and D. C. D'Avanzo, "Large-signal HBT model with improved collector transit time formulation for GaAs and InP technologies," in *IEEE MTT-S Int. Microw. Symp. Dig.*, 2003, pp. 635–638.

[16] I. Angelov, K. Choumei, and A. Inoue, "An empirical HBT large-signal model for CAD," *Int. J. RF Microwave CAE*, vol. 13, pp. 518–533, Nov. 2003.

[17] M. Rudolph, R. Doerner, and P. Heymann, "Direct extraction of HBT equivalent circuit elements," *IEEE Trans. Microw. Theory Tech.*, vol. 47, no. 1, pp. 82–84, Jan. 1999.

[18] J. Hilsenbeck, F. Lenk, W. Heinrich, and J. Würfl, "Low phase noise MMIC VCOs for Ka-band applications with improved GaInP/GaAs-HBT technology," in *IEEE GaAs IC Symp. Dig.*, 2003, pp. 223–226.

[19] F. Lenk and M. Rudolph, "New extraction algorithm for GaAs-HBTs with low intrinsic base resistance," in *IEEE MTT-S Int. Microw. Symp. Dig.*, 2002, pp. 725–728.

[20] FBH HBT Model. [Online]. Available: http://www.fbh-berlin.de/modeling.html

[21] UCSD HBT Model Equations. [Online]. Available: http://hbt.ucsd.edu/

[22] C.-J. Wei, J. M. Gering, and Y. A. Tkachenko, "Enhanced high-current VBIC model," *IEEE Trans. Microw. Theory Tech.*, vol. 53, no. 4, pp. 1235–1243, Apr. 2005.

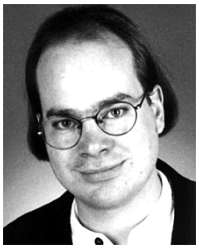

Matthias Rudolph (M'99) was born in Stuttgart, Germany, in 1969. He received the Dipl.-Ing. degree in electrical engineering from Technische Universität Berlin, Berlin, Germany, in 1996, and the Dr.-Ing. degree from Technische Universität Darmstadt, Darmstadt, Germany, in 2001.

He is a Research Scientist at the Ferdinand-Braun-Institut für Höchstfrequenztechnik, Berlin. His research focuses on characterization and modeling of FETs and HBTs and on the design of broadband and low-noise amplifiers.

Ralf Doerner (M'97) was born in Neindorf, Germany, in 1965. He received the Dipl.-Ing. degree in communications engineering from the Technische Universität Ilmenau, Ilmenau, Germany, in 1990.

Since 1989, he has been working on microwave measuring techniques. In 1992, he joined the Ferdinand-Braun-Institut für Höchstfrequenztechnik, Berlin, Germany. His current research is focused on calibration problems in on-wafer millimeter-wave measurements of active and passive devices and circuits and on nonlinear characterization of microwave power transistors.